Nonlinear PDE-Based control of the electron temperature in H-mode tokamak plasmas

H Mameche, Emmanuel Witrant, Christophe Prieur

Nonlinear PDE-Based control of the electron temperature in H-mode tokamak plasmas

H. Mameche, E. Witrant and C. Prieur

***Abstract*— This paper studies the exponential stability of the electron temperature profile in H-mode tokamak plasmas. Lyapunov stability analysis is carried in an infinite-dimensional setting on the nonlinear partial differential equation describing the dynamics. The nonlinear components are handled with the sum of squares framework, in order to prove the exponential convergence of the Lyapunov function. Nominal stability of the system is first checked, then a controller is proposed to improve the convergence rate of the closed-loop system. The controller algorithm including the input constraints is then used for profile tracking on the RAPTOR simulator with different challenging scenarios.**

I. INTRODUCTION

The overall objective of controlling the plasma in tokamaks is to steer it towards a desired operation point defining a plasma scenario. A baseline for high-performance scenarios for tokamaks is H-mode (High confinement mode), where the plasma is strongly heated, exceeding a threshold above which the transport of plasma energy in the edge area is reduced and results in a transport barrier. In this mode, the energy confinement time is significantly enhanced, typically by a factor of 2 or more [1]. To reach and maintain these high-performance scenarios, plasma profiles control plays a fundamental role. These profiles are: magnetic radial profiles (such as the poloidal magnetic flux $\Psi(x)$, the safety factor $q(x)$ or its inverse $\iota(x)$, where x is the location along the small plasma radius), and kinetic profiles, such as electrons and ions temperature and density. These are spatially distributed profiles with two-time scales coupled nonlinear dynamics, hence the difficulty of the control problem. Different approaches have been made to tackle these difficulties. In [2] and following works, a two-time scale linearized data-driven model was built based on singular perturbations theory, and was used to control the poloidal magnetic flux $\Psi(x)$ and the safety factor $q(x)$ in [3]. Other works use first-principles-driven models that capture the dominant and relevant dynamics to synthesize the controller as in [4] [5]. Taking into account the spatially distributed nature of the dynamics, [6] used a spatially discretized model for current profile control, while other works used infinite dimensional theory to synthesize the control algorithms as in [7].

While some previous works emphasized on the coupling between the dynamics and used a linearized model as in [8] and the experimental validation in [9], we are interested in the nonlinearity of the dynamics. In this tokamak control perspective, control of nonlinear PDEs is a recent and challenging topic. An interesting way to tackle the problem is to separate a "slow" finite set of eigenvalues of the system operator that capture the dominant dynamics, and use it as a basis to synthesize the finite-dimensional controller [10]. But in the case of nonlinear parabolic PDEs, a precise approximation of the dynamics may lead to a large number of modes that should be included [11], and this is what motivates us to choose the infinite-dimensional framework to tackle the problem. As in [7], we use a Lyapunov control function approach to synthesize the controller that increases the convergence rate of the closed-loop system.

This paper is organized as follows: in Section II, we present the dynamical model for the electron temperature profile including the transport model modification to represent the H-mode pedestal. In Section III, we use the direct Lyapunov method for the stability analysis of the PDE, then we use the Sum of Squares framework to verify the positivity of the differential matrix inequalities emerging from the Lyapunov analysis to check the nominal stability of the system. We then propose a control algorithm to increase the convergence rate of the closed-loop system. Finally, in Section IV we use the RAPTOR simulator [5] to evaluate the control strategy including the input constraints.

The main variables definitions are given in Table I.

II. SYSTEM DESCRIPTION AND CONTROL PROBLEM

A. Electron temperature dynamics

In this study we focus on the electron temperature T_e dynamics, modeled by a diffusion equation under the infinite cylinder geometry hypothesis (the transport is symmetric in the toroidal and the poloidal directions). The only space variable is the cylinder radius ρ and $x = \rho/a$ is the normalized radial variable (a is the small plasma radius). The transport dynamics is modeled as:

$$\frac{3}{2}\frac{\partial(n_e T_e)}{\partial t} = \frac{1}{a^2}\frac{1}{x}\frac{\partial}{\partial x}(x n_e \chi_e \frac{\partial T_e}{\partial x}) - P_{sinks} + P_{sources}, \quad (1)$$

with boundary and initial conditions: $\frac{\partial T_e}{\partial x}(0,t) = 0$, $T_e(1,t) = T_{e,edge}(t), \forall t \geq t_0$ and $T_e(x,t_0) = T_0(x), \forall x \in [0,1]$.

In this model, $n_e(x,t)$ is the electron density, $\chi_e(x,t)$ is the electron heat diffusivity, $T_{e,edge}(t)$ is the edge temperature and $P_{sources}(x,t) = P_{OH}(x,t) + P_{aux}(x,t)$ is the supplied heating power density. $P_{OH}(x,t)$ is the power density due to

The authors are with Univ. Grenoble Alpes, CNRS, Grenoble INP, GIPSA-lab, 38000 Grenoble, France. Email: {hamza.mameche, emmanuel.witrant, christophe.prieur}@gipsa-lab.fr.

TABLE I

RELEVANT PHYSICAL VARIABLES DEFINITION

Variable	*Description*	*Unit*
a	small plasma radius	m
R	major plasma radius	m
B_ψ	poloidal magnetic field	T
B_ϕ	toroidal magnetic field	T
B_{ϕ_0}	toroidal magnetic field at the center	T
I_p	total plasma current	A
n_e	electron density profile	m^{-3}
n_i	ion density profile	m^{-3}
p_e	electron pressure profile	eVm^{-3}
P_{OH}	ohmic power density	W/m^3
P_{aux}	auxiliary sources power density	W/m^3
T_i	ions temperature profile	eV
T_e	electrons temperature profile	eV
x	normalized spatial variable	
e	electron charge, 1.6022×10^{-19}	C
m_e	electron mass, 9.1096×10^{-31}	kg
Ψ	poloidal magnetic flux	$T/m2$
Φ	toroidal magnetic flux	$T/m2$
q	safety factor	
s	magnetic shear	
V'	$V':=\frac{\partial V}{\partial\rho}$, and V is the volume of a ρ surface	m^2
ι	inverse of the safety factor	
χ_e	electron diffusivity	m^2/s
ρ	spatial variable along the small plasma radius	m
ρ^*	electron gyroradius	m
τ_E	global energy confinement time	s

ohmic effect and $P_{aux}(x,t)$ is the auxiliary heating sources. $P_{sinks}(x,t)$ represents the lost power density such as electron-ion equipartition losses $P_{ei}(x,t)$ and radiation losses, and is neglected as in [5].

B. Electron heat diffusivity model

Because of the complexity of the heat transport dynamics, there is no fully analytic model for the heat diffusivity model. Instead, semi-empirical models have been proposed and tested on experimental data. We choose to use the modified bohm/gyrobohm model in [12] for χ_e:

$$\begin{cases} \chi_e = \chi_{e_c}\times f_s, \quad \chi_{e_c} = (2\chi_{Be}+\chi_{gBe})f_s, \\ \chi_{Be} = 4\times10^{-5}R\left|\frac{\nabla(n_eT_e)}{n_eB_{\phi_0}}\right|q^2\left(\frac{T_{e,0.8}-T_{e,1.0}}{T_{e,1.0}}\right), \\ \chi_{gBe} = 5\times10^{-6}\sqrt{T_e}\left|\frac{\nabla T_e}{B^2_{\phi_0}}\right|, \\ f_s = \frac{1}{1+k\left(\frac{\omega_{E\times B}}{\gamma_{TG}}\right)^2}\times\frac{1}{max(1,(s-s_{thres})^2)} \end{cases} \tag{2}$$

where, χ_{e_c} is the classical bohm/gyrobohm model, χ_{Be} is the Bohm diffusivity, χ_{gBe} is the gyro-Bohm diffusivity. B_{ϕ_0} is the toroidal magnetic field at the center, R is the major radius, q is the safety factor and $T_{e,0.8}$ represents the electron temperature at $x=0.8$ and $T_{e,1.0}$ at $x=1$. The term $((T_{e,0.8}-T_{e,1.0})/T_{e,1.0})$ tackles the non-local dependence by representing the phenomena in which the diffusivity increases when the edge temperature is decreased, and vice versa. s is the magnetic shear, $\omega_{E\times B}$ is the flow shearing rate, γ_{ITG} is the growth rate of ion temperature gradient (ITG), and k a coefficient.

In order to represent the *pedestal* behaviour corresponding to the H-mode, the classical Bohm/gyro-Bohm model χ_{e_c} is then multiplied by f_s: the suppression function for the electron thermal diffusivity. In f_s, the first term represents the flow shearing rate through $\omega_{E\times B}$ and the reduction of the turbulence growth rate through the growth rate of ion temperature gradient γ_{ITG} [13]. The second term reduces the transport only in the region where the magnetic shear s exceeds a specified threshold s_{thres}. To simplify the incorporation of this modification to the diffusivity model, the suppression function f_s was taken as polynomial approximation of the experimental results obtained in [12].

C. Control problem

To formulate our control system from the electron temperature dynamics in II-A and II-B, we consider these assumptions:

Assumption 1. Because of the slow and small time variations of the q profile compared to the T_e one, and in order to decouple the two dynamics in χ_{Be} (2), we choose q as a time-averaged polynomial approximation of a nominal $q(x,t)$ profile simulated in RAPTOR. Similarly, L_{T_e} is a time average for $((T_{e,0.8}-T_{e,1.0})/T_{e,1.0})$ in (2), and n_e is taken as a time-fixed, line-averaged density $\bar{n}_e$ which is a classical variable for tokamaks, this assumption is made to focus on the electron temperature dynamics and its nonlinear coupling with the electron heat diffusivity.

Assumption 2. To deal with the terms with absolute value in χ_{Be} and χ_{gBe} (2), we assume that $\frac{\partial T_e}{\partial x}\leq 0$ almost always and everywhere. This assumption is verified experimentally given that auxiliary power sources target mainly the central region ($x\leq x_{inv}$), and act with a wide angle when deposited on the core region ($x_1\leq x\leq x_{ped}$), ($x_{inv}\approx0.45$ and $x_{ped}\approx0.9$ in TCV tokamak H-mode plasmas [14]). We also assume that $T_{e,edge}$ is very small compared to the temperature in the center of the plasma and we can consider it as zero.

We get the control system described by a nonlinear diffusion PDE:

$$\frac{\partial T_e}{\partial t} = \frac{A}{x}\frac{\partial}{\partial x}\left(x\left(B(x)+C(x)\sqrt{T_e}\right)\left(\frac{\partial T_e}{\partial x}\right)^2\right)+u, \quad \forall x\in[0,1] \tag{3}$$

with boundary conditions,

$$\frac{\partial T_e}{\partial x}(0,t)=0,\ T_e(1,t)=0,\forall t\geq t_0 \tag{4}$$

where: $A=\frac{2}{3a^2}$, $B(x)=\frac{-8\times10^{-5}RL_{T_e}}{B_{\phi_0}}q^2(x)f_s(x)$, $C(x)=\frac{-5\times10^{-6}}{B^2_{\phi_0}}f_s(x)$.

The control problem is to prove the nominal stability of an arbitrary equilibrium point $(\bar{u}(x),\bar{T}_e(x))$ of the system (3)-(4), and to synthesize a control strategy to ensure the tracking of a reference electron temperature profile $T_{e,ref}$.

III. STABILITY ANALYSIS AND DISTRIBUTED CONTROL

A. Stability of the open-loop system

In this section, we develop a Lyapunov function for the nonlinear diffusion PDE in (3)-(4) to prove the nominal

stability of the equilibrium $(\bar{u}(x), \bar{T}_e(x))$. To do that, we consider the following Lyapunov function candidate:

$$V_1(T_e) = \frac{1}{2}\int_0^1 x P_{T_e}(x)(T_e - \bar{T}_e)^2 \, dx \tag{5}$$

where $\bar{T}_e$ is the steady-state equilibrium resulting from a constant input $\bar{u}$. $P_{T_e}(x)$ is a weighting function with $P_{T_e}(x) > 0$ for all $x \in [0,1]$ to ensure the positivity of $V_1(T_e)$. The Lyapunov function candidate is $(xP_{T_e}(x))$-weighted $\mathscr{L}^2([0,1])$ norm squared. We multiply by x to handle the singularity at $x = 0$ when we differentiate $V_1(T_e)$. Using a similar development as in [15], we present the main result of the paper.

Theorem 1: Suppose that for a given positive number α_1, there exist a polynomial $P_{T_e}(x)$ and a 5×5 symmetric polynomial matrix $H(x)$, such that $P_{T_e}(x) > 0$ for all $x \in [0,1]$, $H(0) \geq 0$, $H_{1,1}(1) \leq 0$ and:

$$F(x) + \bar{H}(x) \geq 0, \quad \forall x \in [0,1] \tag{6}$$

where $F(x) + \bar{H}(x)$ is defined in (8) and its elements are defined in (9).

Then the time derivative $\dot{V}_1$ of V_1 defined in (5) along the solutions of (3)-(4) verifies:

$$\dot{V}_1(T_e) \leq -\alpha_1 V_1(T_e) + \int_0^1 x P_{T_e}(x)(T_e - \bar{T}_e)\tilde{u} \, dx \tag{7}$$

where $\tilde{u}$ is defined as $\tilde{u} = u - \bar{u}$.

$$F(x) + \bar{H}(x) = \left[\begin{array}{cccccc|cc}
f_9 + h_1 & h_2 & h_3 & f_7 + h_4 & h_5 & 0 & | & \\
\bullet & f_7 + h_{10} & h_{11} & h_{12} & h_{13} & 0 & | & \\
\bullet & \bullet & 0 & h_{18} & 0 & 0 & | & \\
\bullet & \bullet & \bullet & f_8 + h_{21} & h_{22} & f_5 & | & \\
\bullet & \bullet & \bullet & \bullet & f_5 & 0 & | & \\
\bullet & \bullet & \bullet & \bullet & \bullet & 0 & | & \\
\bullet & \bullet & \bullet & \bullet & \bullet & \bullet & | & \\
\bullet & \bullet & \bullet & \bullet & \bullet & \bullet & | & \\
\bullet & \bullet & \bullet & \bullet & \bullet & \bullet & | & \\
\bullet & \bullet & \bullet & \bullet & \bullet & \bullet & | & \\
\bullet & \bullet & \bullet & \bullet & \bullet & \bullet & | & \\
\bullet & \bullet & \bullet & \bullet & \bullet & \bullet & | & \\
\bullet & \bullet & \bullet & \bullet & \bullet & \bullet & | & \\
\bullet & \bullet & \bullet & \bullet & \bullet & \bullet & | &
\end{array}\right.$$

$$\left.\begin{array}{cccccccc}
h_6 & h_7 & 0 & 0 & f_8 + h_8 & h_9 & f_5 & 0 \\
f_8 + h_{14} & h_{15} & f_5 & 0 & h_{16} & h_{17} & f_6 & 0 \\
h_{19} & f_5 & 0 & 0 & h_{20} & f_6 & 0 & 0 \\
h_{23} & h_{24} & f_6 & 0 & h_{25} & 2h_{27} & f_1 & f_3 \\
h_{26} & f_6 & 0 & 0 & h_{27} & f_1 & f_3 & 0 \\
f_6 & 0 & 0 & 0 & f_1 & f_3 & 0 & 0 \\
h_{28} & h_{29} & f_1 & f_3 & h_{30} & h_{31} & f_2 & f_4 \\
\bullet & f_1 & f_3 & 0 & \frac{3}{4}h_{31} & f_2 & f_4 & 0 \\
\bullet & \bullet & 0 & 0 & f_2 & f_4 & 0 & 0 \\
\bullet & \bullet & \bullet & 0 & f_4 & 0 & 0 & 0 \\
\bullet & \bullet & \bullet & \bullet & h_{32} & h_{33} & 0 & 0 \\
\bullet & \bullet & \bullet & \bullet & \bullet & 0 & 0 & 0 \\
\bullet & \bullet & \bullet & \bullet & \bullet & \bullet & 0 & 0 \\
\bullet & \bullet & \bullet & \bullet & \bullet & \bullet & \bullet & 0
\end{array}\right] \tag{8}$$

Proof: The time derivative of the Lyapunov function (5) along (3)-(4) is:

$$\dot{V}_1(T_e) = \int_0^1 x P_{T_e}(x)\frac{\partial T_e}{\partial t}(T_e - \bar{T}_e) \, dx = \int_0^1 x P_{T_e}(x)(T_e - \bar{T}_e) \times \left\{ \frac{A}{x}\frac{\partial}{\partial x}\left[x\left(B(x) + C(x)\sqrt{T_e}\right)\left(\frac{\partial T_e}{\partial x}\right)^2 \right] + u \right\} dx$$

Integrating $\dot{V}$ by parts we get:

$$\dot{V}_1(T_e) = \left. A P_{T_e}(x)(T_e - \bar{T}_e)\, x\left(B(x) + C(x)\sqrt{T_e}\right)\left(\frac{\partial T_e}{\partial x}\right)^2 \right|_0^1 - \int_0^1 A\frac{\partial (P_{T_e}(x)(T_e - \bar{T}_e))}{\partial x}\left[x\left(B(x) + C(x)\sqrt{T_e}\right)\left(\frac{\partial T_e}{\partial x}\right)^2 \right] dx + \int_0^1 x P_{T_e}(x)(T_e - \bar{T}_e)u \, dx$$

With $m \in \mathbb{N}^*$, define $D^m T_e := \left[T_e, \frac{\partial T_e}{\partial x}, \ \ldots, \frac{\partial^m T_e}{\partial x^m}\right]^T$ a vector of spacial partial derivatives up to order m. Considering the boundary conditions (4) we get:

$$\begin{aligned}
&\dot{V}_1(T_e) + \alpha_1 V_1(T_e) = \\
&-\int_0^1 x A P_{T_e}(x)\left(B(x) + C(x)\sqrt{T_e}\right)\left(\frac{\partial T_e}{\partial x}\right)^3 dx \\
&-\int_0^1 x A P'_{T_e}(x) T_e \left(B(x) + C(x)\sqrt{T_e}\right)\left(\frac{\partial T_e}{\partial x}\right)^2 dx \\
&+\int_0^1 x A (P'_{T_e}(x)\bar{T}_e + P_{T_e}(x)\bar{T}_e{}')\left(B(x) + C(x)\sqrt{T_e}\right)\left(\frac{\partial T_e}{\partial x}\right)^2 dx \\
&+\frac{\alpha_1}{2}\int_0^1 x P_{T_e}(x)(T_e - \bar{T}_e)^2 \, dx + \int_0^1 x P_{T_e}(x)(T_e - \bar{T}_e)(\bar{u} + \tilde{u}) \, dx \\
&= -\int_0^1 G(x, \sqrt{T_e}, D^1 T_e) \, dx + \int_0^1 x P_{T_e}(x)(T_e - \bar{T}_e)\tilde{u} \, dx
\end{aligned} \tag{10}$$

At this stage we perform a change of variable $\tau = \sqrt{T_e}$, to ensure the polynomial dependence of G on the dependent variable and its derivatives. We can then write G in terms of τ as:

$$G(x, D^1\tau) = \xi(D^1\tau)^T F(x)\xi(D^1\tau) \tag{11}$$

where $F(x)$ is defined in (8)-(9) by only taking the f_i elements, and:

$$\xi(D^1\tau) := \left[1, \tau, \frac{\partial\tau}{\partial x}, \tau^2, \tau\frac{\partial\tau}{\partial x}, \left(\frac{\partial\tau}{\partial x}\right)^2, \tau^3, \tau^2\frac{\partial\tau}{\partial x}, \tau\left(\frac{\partial\tau}{\partial x}\right)^2, \left(\frac{\partial\tau}{\partial x}\right)^3, \tau^4, \tau^3\frac{\partial\tau}{\partial x}, \tau^2\left(\frac{\partial\tau}{\partial x}\right)^2, \tau\left(\frac{\partial\tau}{\partial x}\right)^3\right]^T$$

Note that:

$$\int_0^1 \xi(D^1\tau)^T F(x)\xi(D^1\tau) \, dx = \int_0^1 \left[\xi(D^1\tau)^T F(x)\xi(D^1\tau) + \frac{d}{dx}\left(\mu(\tau)^T H(x)\mu(\tau)\right)\right] dx - \left(\mu(\tau)^T H(x)\mu(\tau)\right)\Big|_0^1 \tag{12}$$

where: $\mu(\tau) := \left[1, \tau, \tau^2, \tau^3, \tau^4\right]^T$, and $H(x)$ is a 5×5 symmetric polynomial matrix. Using (12) and since we have that: $\mu(\tau(1)) = [1,0,0,0,0]^T$, we rewrite (10) as:

$$\begin{aligned}
\dot{V}_1(T_e) + \alpha_1 V_1(T_e) = &-\int_0^1 \xi(D^1\tau)^T (F(x) + \bar{H}(x))\xi(D^1\tau) \\
&+ H_{1,1}(1) - \mu(\tau(0))^T H(0)\mu(\tau(0)) + \int_0^1 x P_{T_e}(x)(T_e - \bar{T}_e)\tilde{u} \, dx
\end{aligned}$$

$$f_1 = \tfrac{4}{9}(ABxP'_{T_e}),\ f_2 = \tfrac{2}{3}(ACxP'_{T_e}),\ f_3 = \tfrac{4}{5}(ABxP_{T_e}),\ f_4 = (ACxP_{T_e}),\ f_5 = -\tfrac{4}{9}(ABx(P'_{T_e}\bar{T}_e + P_T\bar{T}_e{}')),$$
$$f_6 = -\tfrac{2}{5}(ACx(P'_{T_e}\bar{T}_e + P_T\bar{T}_e{}')),\ f_7 = \tfrac{1}{3}(\alpha_1 xP_{T_e}\bar{T}_e - xP_{T_e}\bar{u}),\ f_8 = -\tfrac{1}{10}(\alpha_1 xP_{T_e}),\ f_9 = (xP_{T_e}\bar{T}_e\bar{u} - \tfrac{1}{2}\alpha_1 xP_{T_e}\bar{T}_e{}^2).$$
$$h_1 = \tfrac{dH_{1,1}}{dx},\ h_2 = \tfrac{dH_{1,2}}{dx},\ h_3 = H_{1,2},\ h_4 = \tfrac{2}{3}\tfrac{dH_{1,3}}{dx},\ h_5 = H_{1,3},\ h_6 = \tfrac{1}{2}\tfrac{dH_{1,4}}{dx},\ h_7 = H_{1,4},\ h_8 = \tfrac{2}{5}\tfrac{dH_{1,5}}{dx},\ h_9 = H_{1,5},$$
$$h_{10} = \tfrac{2}{3}\tfrac{dH_{1,3}}{dx} + \tfrac{dH_{2,2}}{dx},\ h_{11} = H_{1,3} + H_{2,2},\ h_{12} = \tfrac{1}{2}\tfrac{dH_{1,4}}{dx} + \tfrac{dH_{2,3}}{dx},\ h_{13} = H_{1,4} + 2H_{2,3},\ h_{14} = \tfrac{2}{5}\tfrac{dH_{1,5}}{dx} + \tfrac{dH_{2,4}}{dx},$$
$$h_{15} = H_{1,5} + 3H_{2,4},\ h_{16} = \tfrac{dH_{2,5}}{dx},\ h_{17} = 4H_{2,5},\ h_{18} = H_{1,4} + H_{2,3},\ h_{19} = H_{1,5} + H_{2,4},\ h_{20} = H_{2,5},\ h_{21} = \tfrac{2}{5}\tfrac{dH_{1,5}}{dx} + \tfrac{dH_{3,3}}{dx},$$
$$h_{22} = H_{1,5} + 2H_{3,3},\ h_{23} = \tfrac{dH_{3,4}}{dx},\ h_{24} = 3H_{3,4},\ h_{25} = \tfrac{dH_{3,5}}{dx},\ h_{26} = 2H_{3,4},\ h_{27} = 2H_{3,5},\ h_{28} = \tfrac{dH_{4,4}}{dx},\ h_{29} = 3H_{4,4},$$
$$h_{30} = \tfrac{dH_{4,5}}{dx},\ h_{31} = 4H_{4,5},\ h_{32} = \tfrac{dH_{5,5}}{dx},\ h_{33} = 4H_{5,5}. \tag{9}$$

where $\bar{H}(x)$ is defined in (8)-(9) by only taking the h_i elements in (8) and set the f_i elements to 0.

Then if $H(0) \geq 0$, $H_{1,1}(1) \leq 0$ and $F(x) + \bar{H} \geq 0,\ \forall x \in [0,1]$, we get that:

$$\dot{V}_1(T_e) \leq -\alpha_1 V_1(T_e) + \int_0^1 xP_{T_e}(x)(T_e - \bar{T}_e)\tilde{u}\ dx$$

■

Remark 1. Notice that unsimilarly to [15] where in a system model $\frac{\partial W}{\partial t} = F(x, D^\beta W)$, F is polynomial on its second argument, it is not the case for our model, therefore we had to apply integration by part followed by a change of variable to obtain $G(x, D^1\tau)$ to which we can apply the rest of the procedure.

Remark 2. As a result of the theorem, by setting $\tilde{u} = 0$, we get that the equilibrium $(\bar{u}, \bar{T}_e)$ is exponentially stable in V_1.

B. Calculation of the weighting Function

Since $F(x)$ contains $P_{T_2}(x)$ and its derivative, and $\bar{H}(x)$ contains continuously differentiable functions and their derivatives, (6) is a differential matrix inequality. Using the theorem assumption that $P_{T_e}(x)$ and the elements of $H(x)$ are polynomials in x, it is possible to formulate the positivity of $F(x) + \bar{H}(x)$ in $x \in [0,1]$ as a convex optimization problem in the form of Semidefinite Programming using the following corollary of the Putinar's Positivstellensatz theorem [16]:

Corollary 1.1: If there exists $N(x) \in \Sigma^{14\times 14}[x]$ (Sum Of Squares polynomial matrix of order 14) such that:

$$F(x) + \bar{H}(x) - N(x)x(1-x) \in \Sigma^{14\times 14}[x] \tag{13}$$

then (6) holds.

In this context, the problem of finding $P_T(x)$ is formulated as the following feasibility Sum Of Squares problem (SOSP):

$$\begin{aligned}&Find\ P_{T_e}(x),\ H(x),\ N(x).\ Subject\ to:\\ &P_{T_e}(x) > 0\ in\ [0,1],\ F(x) + \bar{H}(x) - N(x)x(1-x) \in \Sigma^{14\times 14}[x],\\ &N(x) \in \Sigma^{14\times 14}[x],\ H(0) \geq 0, H_{1,1}(1) \leq 0.\end{aligned}$$

This problem is then solved using Yalmip with the Sum Of Squares Module [17], and the resulting $P_{T_e}(x)$ is a decreasing polynomial strictly positive on $[0,1]$.

C. Distributed control

Based on the previous analysis, and to perform reference tracking control, we define the control strategy while ensuring exponential stability of the closed-loop system as follows:

Corollary 1.2: If the conditions of Theorem 1 are verified, we choose the control input $u_{ctrl} = \bar{u} + \tilde{u}$, where $\tilde{u}$ is calculated to verify the equality:

$$\int_0^1 xP_{T_e}(x)(T_e - \bar{T}_e)\tilde{u}\ dx = -\alpha_2 V_1(T_e) \tag{14}$$

with $\alpha_2 > 0$, a tuning parameter. With this control we get:

$$\dot{V}_1(T_e) \leq -(\alpha_1 + \alpha_2)V_1(T_e)$$

and the system (3)-(4) with (14) is exponentially stable in V_1 with convergence rate $\alpha_1 + \alpha_2$. An explicit control law from (14) is the proportional controller: $u_{ctrl} = \bar{u} - \frac{\alpha_2}{2}(T_e - \bar{T}_e)$.

IV. Control implementation and results

Now we aim to implement the control strategy on the RAPTOR simulator with TCV tokamak settings. RAPTOR is a lightweight code used to simulate simplified nonlinear plasma transport physics, and is also used as a real-time state observer for the TCV tokamak. We first show the shape constraints on the input, then we present the RAPTOR configuration used for the simulation, we formulate an optimization problem to find the engineering parameters to apply as inputs to the system, and finally we present the results of the simulation where we test the performance and robustness of the controller by adding disturbances and time-delays.

A. Input constraints

During the beginning of the discharge, the plasma heating comes from the induced plasma current I_p whose time evolution scenario is computed offline and defines the discharge phases (ramp-up, flat-top and rump-down). The plasma current is thus not considered as an input to the system (a feedback loop sets the voltage on the poloidal field coils to generate the desired I_p). On the other hand, the auxiliary heating sources such as Electron Cyclotron Resonance Heating (ECRH), Electron Cyclotron Current Drive (ECCD) and NBI are used for the online distributed control. They are subject to profile shape constraints (see Fig.1), and their power densities are approximated by weighted Gaussian distributions, for the case of ECRH/ECCD antennas, we have for the $i-th$ actuator [5]:

$$P_{aux,i}(x,t) = P_i(t)\frac{e^z}{\int_0^a e^z}V'dx,\ z = \frac{-4(x - x_{dep,i})^2}{w_{dep,i}^2} \tag{15}$$

where w_{dep} is the deposit width and x_{dep} is the location of the peak of the deposit. In most cases the x_{dep} and w_{dep} are fixed, and the amplitude of the power density for the i-th actuator $P_i(t)$ in (15) is used as an input in the model and:

$$P_{aux}(x,t) = \sum_i P_{aux,i}(x,t) \tag{16}$$

B. RAPTOR configuration

We use a configuration where the plasma current ramps up from 80 kA to 120 kA and we use two EC antennas as auxiliary sources, with power amplitude $P_1(t)$ and $P_2(t)$, The first one is a pure ECRH heating source deposited at $x_{dep} = 0$ with deposition angle of $w_{dep} = 0.35$, and the second one is an EC current drive (ECCD) source with $x_{dep} = 0.4$ and $w_{dep} = 0.35$. The engineering inputs $P_1(t)$ and $P_2(t)$ are limited to 1 MW.

For the heat diffusivity χ_e we choose the model introduced in [14] (equation (13)), with the parameters used in the paper to fit experimental measurements of the T_e profile in H-mode TCV plasma. In Fig 2 we show a RAPTOR simulation of the T_e profile in H-mode TCV plasma, where we notice the pedestal at the edge.

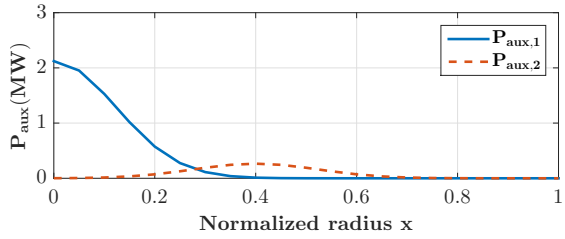

Fig. 1. Auxiliary ECRH ($P_{aux,1}$) and ECCD ($P_{aux,2}$) sources distributions.

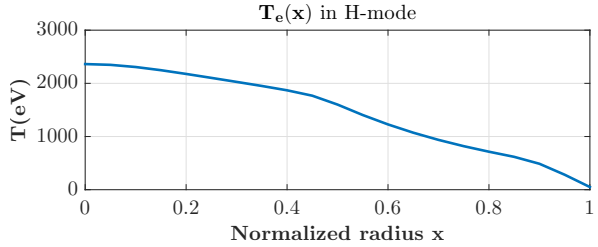

Fig. 2. H-mode simulations of $T_e(x)$ in RAPTOR.

C. The control algorithm

Taking into consideration the constraints on the actuators, we are not able to implement the control algorithm presented in Corollary 1.2. A practical implementation that we use is to calculate and apply at each time step the actuator inputs $u_{ac} = [P_1, P_2]^T$ that solve the squared difference minimization problem of (14):

$$u^*_{ac} = \underset{u_{ac}}{arg\,min} \int_0^1 \Big[xP_{T_e}(x)\Big((P_{aux}(u_{ac}) - u_{ref}) + \frac{\alpha_2}{2}(T_e - T_{e,ref})\Big)\Big]^2 dx \tag{17}$$

subject to: $0 \le P_1 \le 1\text{MW},\ 0 \le P_2 \le 1\text{MW}$.

where $(T_{e,ref},\ u_{ref})$ are the reference temperature profile and its corresponding input, that is the imposed equilibrium point of the system in closed loop with the controller (14).

D. Simulation results

We now present the simulation results with different scenarios in order to test the performance and the robustness of the control algorithm, and we compare the open-loop and the closed-loop responses. To test the behaviour of the controller when changing the operating point we used a 2-stage reference profile.

1) Adding disturbance: The controller disturbance attenuation is tested by adding a third ECCD source at $x_{dep} = 0.2$ with $w_{dep} = 0.35$ and $P_3 = 0.1$ MW at $t = 0.2$ s. The results are shown in Fig. 3, where we see the time evolution of the T_e profile in various space points, as well as the time evolution of u_{ac} that solves the optimization problem (17). We see that the tracking performance in closed loop is significantly improved compared to the open-loop case. The time response in closed loop is further reduced in the region where the actuators are most efficient ($x_{dep} = 0$ and $x_{dep} = 0.4$). Before $t = 0.2$ we see that the optimization routine retrieved the original values $P_1 = 0.3$ MW and $P_2 = 0.3$ MW with a short saturation, and after $t = 0.2$ we can notice that the controller could not totally compensate the effect of the disturbance due to the fact that the disturbance source is not collocated with the input ones.

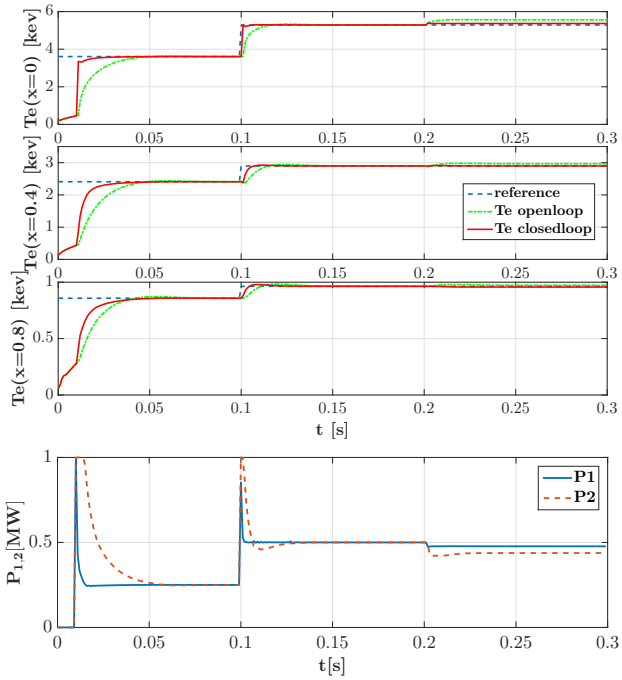

Fig. 3. T_e tracking and time-evolution of $P_{1,2}$ when changing the set point and introducing a disturbance at $t = 0.2$ s.

In Fig. 4, we show a comparison of the time evolution of the Lyapunov function in open loop and closed loop. We can see that the practical implementation of the controller

succeeded to improve the convergence rate.

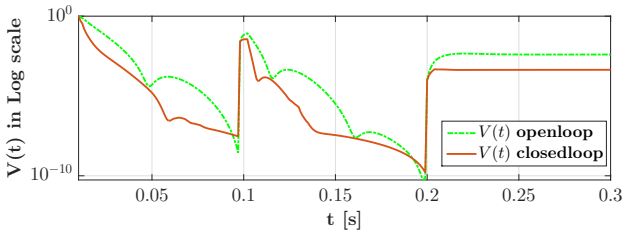

Fig. 4. Open-loop and closed-loop convergence rates of the Lyapunov function.

2) Adding time-delays: Because of the fast dynamics of the system, the computation and the transportation of the control signal is considered as a time-delay. To take it into account we include a time-delay of 5 *ms* in the control loop. In Fig. 5 we see the deterioration of the performance in presence of such time-delay. The time-delay induces an overshoot in the closed-loop response, more important in the plasma centre (where there is more actuation) but which stays within reasonable bounds. The proposed control strategy is thus reasonably robust to time-delays.

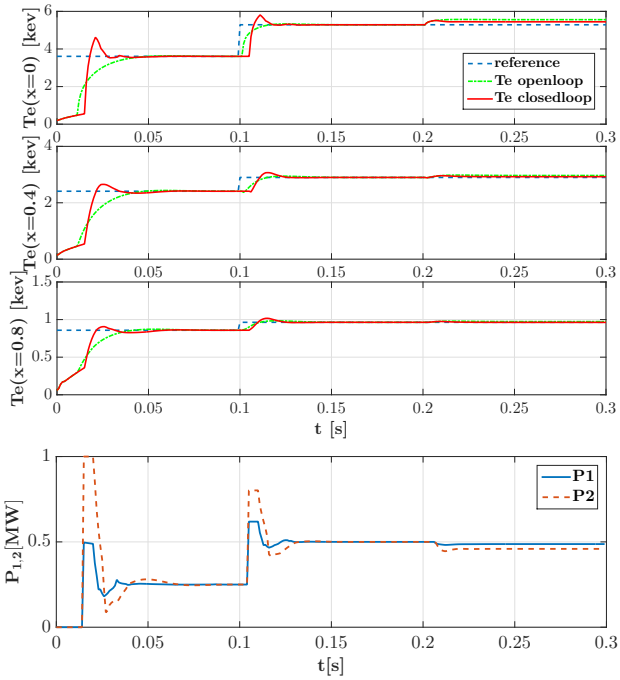

Fig. 5. T_e tracking and time-evolution of $P_{1,2}$ when changing the set point and introducing a disturbance at $t = 0.2$ s in the presence of an input time-delay of 5 ms.

V. Conclusion

In this work, the stability analysis and control of the electron temperature profile in H-mode tokamak plasmas was addressed, with dynamics described by a first-principle control-oriented model.

The stability of the resulting nonlinear parabolic PDE was studied with the Lyapunov approach. The sum of squares framework was used to compute the weighting functions that ensure the positivity of the resulting integral inequalities.

A control strategy was proposed to ensure a good tracking of the electron temperature profile in closed loop at an increased convergence rate. To evaluate the control strategy, RAPTOR plasma simulator was used and the control input constraints were taken into account to derive the engineering control parameters. The simulation results show a good performance of the controller in tracking the H-mode TCV plasma electron temperature profile. The robustness of the controller was investigated with respect to input disturbances and by adding an time-delay.

References

[1] M. Keilhacker, "H-mode confinement in tokamaks," *Plasma Physics and Controlled Fusion*, vol. 29, no. 10A, p. 1401, 1987.

[2] D. Moreau, D. Mazon, M. Ariola *et al.*, "A two-time-scale dynamic-model approach for magnetic and kinetic profile control in advanced tokamak scenarios on JET," *Nuclear Fusion*, vol. 48, no. 10, p. 106001, 2008.

[3] D. Moreau, M. L. Walker, J. R. Ferron *et al.*, "Integrated magnetic and kinetic control of advanced tokamak plasmas on DIII-D based on data-driven models," *Nuclear Fusion*, vol. 53, no. 6, p. 063020, 2013.

[4] E. Witrant, E. Joffrin, S. Brémond *et al.*, "A control-oriented model of the current profile in tokamak plasma," *Plasma Physics and Controlled Fusion*, vol. 49, no. 7, p. 1075, 2007.

[5] F. Felici, "Real-time control of tokamak plasmas: from control of physics to physics-based control," *Ph. D. dissertation, Ecole Polytechnique Fédérale de Lausanne EPFL*, 2011.

[6] M. D. Boyer, J. Barton, E. Schuster *et al.*, "First-principles-driven model-based current profile control for the DIII-D tokamak via LQI optimal control," *Plasma Physics and Controlled Fusion*, vol. 55, no. 10, p. 105007, 2013.

[7] F. Bribiesca Argomedo, E. Witrant, C. Prieur *et al.*, "Lyapunov-based distributed control of the safety-factor profile in a tokamak plasma," *Nuclear Fusion*, vol. 53, no. 3, p. 033005, 2013.

[8] B. Mavkov, E. Witrant, and C. Prieur, "Distributed control of coupled inhomogeneous diffusion in tokamak plasmas," *IEEE Transactions on Control Systems Technology*, no. 99, pp. 1–8, 2017.

[9] B. Mavkov, E. Witrant, C. Prieur *et al.*, "Experimental validation of a Lyapunov-based controller for the plasma safety factor and plasma pressure in the TCV tokamak," *Nuclear Fusion*, vol. 58, no. 5, p. 056011, 2018.

[10] P. D. Christofides, *Nonlinear and robust control of PDE systems: Methods and applications to transport-reaction processes*. Boston, MA, USA: Birkhäuser Basel, 2001.

[11] P. D. Christofides, "Control of nonlinear distributed process systems: Recent developments and challenges," *AIChE Journal*, vol. 47, no. 3, pp. 514–518, 2001.

[12] Y. Pianroj and T. Onjun, "Simulations of H-mode plasmas in tokamak using a complete core-edge modeling in the BALDUR code," *Plasma Science and Technology*, vol. 14, no. 9, p. 778, 2012.

[13] M. Sugihara, Y. Igitkhanov, G. Janeschitz *et al.*, "Simulation studies on H-mode pedestal behavioru during type-I ELMs under various plasma conditions," in *Proceedings of the 28th EPS Conference on Controlled Fusion and Plasma Physics, Funchal, Portugal*, 2001, pp. 629–632.

[14] D. Kim, A. Merle, O. Sauter *et al.*, "Simple predictive electron transport models applied to sawtoothing plasmas," *Plasma Physics and Controlled Fusion*, vol. 58, no. 5, p. 055002, 2016.

[15] G. Valmorbida, M. Ahmadi, and A. Papachristodoulou, "Stability analysis for a class of partial differential equations via semidefinite programming," *IEEE Transactions on Automatic Control*, vol. 61, no. 6, pp. 1649–1654, 2016.

[16] G. Valmorbida, M. Ahmadi, and A. Papachristodoulou, "Semi-definite programming and functional inequalities for distributed parameter systems," in *53rd IEEE conference on decision and control*. IEEE, 2014, pp. 4304–4309.

[17] J. Löfberg, "YALMIP: A toolbox for modeling and optimization in MATLAB," in *Proceedings of the CACSD Conference*, vol. 3. Taipei, Taiwan, 2004.